Received: 18 September 2018 | Revised: 26 March 2019 | Accepted: 27 March 2019

DOI: 10.1002/dvdy.34

RESEARCH ARTICLE

Developmental Dynamics WILEY

3D morphological analysis of spiral intestine morphogenesis in the little skate, *Leucoraja erinacea*

Nicole A. Theodosiou | **Emmanuela Oppong**

Department of Biological Sciences, Union College, Schenectady, New York

Correspondence
Nicole A. Theodosiou, Department of Biological Sciences, Union College, 807 Union Street, Schenectady, NY 12308.
Email: theodosn@union.edu

Funding information
NSF-MRI, DBI, Grant/Award Number: 153185; NSF-MRI, CMMI, Grant/Award Number: 1337768

Abstract

Background: The evolution of organ asymmetries is less explored than the field of organ morphology and coiling. The digestive tract of elasmobranchs provides a fascinating model for studying the evolution of morphological asymmetries. Unique to elasmobranchs and all basal fishes is the spiral intestine, which may represent an intermediate morphology in evolution from the straight gut of lamprey to the elongated coils of higher vertebrates. The short spiral allows for a large absorptive surface area that can fit into a restrictive abdominal space.

Results: Using histology and high resolution microCT, we provide the first 3D morphometric analysis of the spiral intestine during development in the little skate, *Leucoraja erinacea*. Spiral formation is initiated by asymmetric growth in the mesenchyme, causing a bulging fold that protrudes into the lumen of the gut. As development proceeds, the fold elongates and spirals into a right-handed helix. Spiraling progresses along the anterior-posterior axis and is likely the result of mechanical forces driven by the asymmetric growth of surrounding tissues. After initial asymmetric growth, radial constraints from within the gut tube create constrictive forces further propagating spiraling.

Conclusion: We propose a model for potential biophysical mechanisms that direct the morphogenesis of the spiral intestine.

KEYWORDS

elasmobranch, gut looping, *Leucoraja erinacea*, MicroCT, organ chirality, spiral intestine

1 | INTRODUCTION

The conserved chirality of visceral organs speaks to the crucial role asymmetries play during development and evolution. Asymmetries are found in morphologies of organs such as the heart, where the left and right sides are built for different pumping capacities. Asymmetries are also illustrated in the placement of organs within the body, marked by the liver on the right and stomach on the left. Situs solitus, the asymmetric arrangement of organs in an otherwise bilaterially symmetric animal is conserved, and supports the idea that the placement of organs within the body must be crucial for organ function.[1] In humans, complete mirror image rearrangement of organs, or situs inversus, is rare, occurring in 1/10000 live births with little clinical presentation. Single organ inversion, such as dextrocardia, or randomization of organs, heterotaxia have increased cardiac defects and complications.[2,3] Rotation and coiling of the gastrointestinal (GI) tract is regulated to optimize nutrient absorption and prevent malfunctions. Malrotation of the GI tract during development occurs more frequently (1/500) and can lead to twisting and obstruction of the bowels, or volvulus.[4–6] Asymmetric growth, patterning and positioning of organs and tissues within the body is initiated early in the embryo.[7]

Regulating looping of the gut initially by Nodal signaling and later by bone morphogenetic protein signaling is required for careful packaging of the intestines in the body cavity.[8] Looping is important to preserve function, as the length of the GI tract exceeds the body length of an organism. Variability in the length of the intestine is required to increase absorptive surface area so that nutrients can be absorbed. The length of the intestines corresponds with diet, with herbivores requiring more time for cellulose break down. Carnivores have a 3:1 ratio between the GI tract and length of body axis, while this ratio increases to 6:1 for omnivores and 10:1 in herbivores.[9] Of interest, invertebrates such as the snail also have a gut length that exceeds body length. Nodal's presence in mollusks and role in patterning spiral cleavage point to the evolutionary significance of morphological asymmetries.[10,11] Thus, controlled looping of the GI tract likely appeared as one of the first asymmetric events in evolution.[12]

In contrast to animals with GI tracts many times the length of their bodies, basal fishes have GI tracts that closely match the length of the main body axis. This is due to the fact that basal fish have short intestines that form an internal spiral valve. The structure of the spiral valve intestine allows for a large absorptive surface area encased within a short run of intestine.[13] It is believed that this more compact structure stems from the restricted coelomic cavity found in early fishes.[14,15] For example, in sharks the liver required for buoyancy can take up to 25% of its body weight and thus encompasses most of the body cavity.[16] The spiral valve intestine is unique to all basal fishes including the lamprey of the jawless superclass Agnatha, the jawed cartilaginous fishes Chondrichthyes, and the sarcopterygians (including coelacanths, lungfish) of the Octeichthyes.[17] Additionally, recent fossil evidence from early nonteleost actinopterygians has verified the early appearance of the spiral intestine, speaking to its omnipresence in all basal fishes.[18] Teleosts, however, lack a spiral valve intestine. Thus, the spiral intestine represents an early feature in the evolution of vertebrates and provides a great model for investigating the evolution of morphological asymmetries.

Along with its evolutionary importance, the spiral intestine is of interest for several reasons. Initial studies in the little skate *Leucoraja erinacea* have demonstrated that the spiral intestine is divided into functionally and histologically distinct regions, not dissimilar to the regions of the extended intestines found in higher vertebrates.[19] Most of the spiral intestine, the anterior or rostral and mid-regions, are lined with villi reminiscent of a small intestine, while the caudal-most region contains a flattened epithelium with a high density of acid-mucin producing goblet cells, more similar to a colon. The caudal region expresses the colon-specific water channel AQP4, and has an increased rate of water absorption, further corroborating that this region may be a rudiment of the colon.[20] In addition, the developing skate intestine expresses the colon genes *Hoxd13* and *Hoxa13* in a pattern similar to that seen in the chick.[19] Further understanding of the formation of the spiral intestine will help make the link to understand how patterning genes can give rise to morphologically distinct organs in diverse animals.

The spiral itself is a unique structure. The growth and developmental of spirals have been studied in the context of cleavage in snails and growth in plant tendrils.[21,22] As demonstrated in these models, spirals may arise by asymmetric growth or planar rotation. Alternatively, spirals can be considered a result of mechanical forces during development. Differential growth can result in residual stress within tissues.[23] When compressive residual stress exceeds a critical value, released potential energy can cause buckling of adjacent tissues forming creases and folds.[24,25] An example of this is during villification of the intestine, in which smooth muscle-driven compression results in buckling of the epithelium to form villi.[26] Similar forces can also be achieved by differential growth of two adjacent tissues. Initial looping of the gut is the result of cell shape changes in the attached dorsal mesentery that rotate the gut.[27,28] As the embryonic gut tube continues to grow and elongate relative to the dorsal mesentery, subsequent looping of the gut occurs by mechanical buckling that results from a differential growth-driven mechanism.[29]

In this study, we examine the development of the spiral within the gut tube of the little skate, *Leucoraja erinacea* by using histology, high resolution microCT scans, and 3D morphometry. Anatomical analysis of the emergence of the spiral during skate intestinal development represents an important first step in identifying the molecular and biophysical mechanisms by which morphogenesis of this structure occurs.

2 | RESULTS

Here, we describe the development of the internal spiral in the intestine of the little skate *Leucoraja erinacea.* Little skate embryos reach maturation over 11 months when maintained at 16°C. An asymmetric bulge appears in the enclosed gut tube at stage 25, and we track development of the different tissue layers of the gut to prehatching, stage 34. Morphometric analysis of the spiral between stages 25 and 34 reveals the role that constraining forces likely act on the intestine to shape the spiral during development.

2.1 | Histology of the developing spiral intestine

To determine a framework for tissue differentiation and the process of spiral formation, we first examined gut development from stage 24 to prehatching (stage 34). The stage 24 embryonic gut tube is completely symmetric, and the cells originating from the endoderm and splanchnic mesoderm are

indistinguishable (n = 4; Figure 1A). At stages 24 and 25, the gut tube is continuous with the umbilicus, with the umbilicus not yet narrowed to a distinct tube (Figure 1C). Transverse sections through the stage 25 embryonic gut reveal an inner endoderm-derived epithelium surrounded by several players of mesenchymal cells (n = 7; Figure 1D). A dense group of mesenchyme cells creates a bulge into the lumen of the gut, giving the lumen a crescent shape. The asymmetric protrusion into the lumen appears to rotate relative to the dorsal mesentery, depending on the rostral-caudal position along the intestine (Figure 1D-D″, arrowheads).

The effect is that the lumen emerges in either U, J, or C-shapes (Figure 1D, D′, D″, respectively). As the first discernable break in symmetry, we believe this bulge or protrusion at stage 25 marks the initiation of the spiral fold in the intestine. To determine if the break in symmetry is due to changes in cell number or shape, the density of mesenchymal cells on either side of the crescent-shaped endoderm was measured at different rostral-caudal positions in the intestine (Figure 1B′). The inner curvature has a mean density of 27 cells/$10^3\mu m^2$, significantly higher than the mean density of the outer curvature at 20.4 cells/$10^3\mu m^2$ (n = 9; $P = 0.003$). The ratio of mesenchymal cell densities between the inner and outer curvature is 1.3.

By stage 27, the ventral body wall and gut tube have closed, and a distinct umbilicus is visible extending from the gut (Figure 1E). The gut tube has grown in diameter with the endoderm appearing as a pseudostratified epithelium with a visible basement membrane (n = 5; Figure 1F,F′).[30] The inner bulge of cells making up the initial spiral fold has expanded, maintaining the crescent-shaped lumen. The surrounding mesenchyme cells do not yet appear to be organizing into different layers (Figure 1F′).

Differentiation of the different tissue layers within the spiral intestine is distinct by stage 30 (n = 6; Figure 1H,H′). Compared with earlier stages, the pseudostratified columnar epithelium has thinned and the protrusion into the lumen is now an extended fold that turns inward to form a spiral. For simplicity, we refer to the cells that enclose the spiral within the gut tube as the outer casing (Figure 3G). The outer casing at stage 30 contains submucosa and muscularis regions (Figure 1H′). Before hatching at stage 34, the spiral fold has continued to increase in length, turning inward on itself 2-fold, with villi present on all epithelial surfaces (n = 3; Figure 1J). High magnification reveals clearly organized villi with a lamina propria and differentiated muscle fibers (Figure 1J′).

2.2 | MicroCT scans and reconstructions of the developing spiral intestine

To better visualize and trace the progression of spiral formation in the developing skate intestine, we used 3D reconstructions of microCT scans. It is noteworthy that spiral formation visualized by microCT matches the morphology of spiral formation observed by histology (Figures 1 and 2). Initially, the mesenchyme forms a protrusion into the lumen at stage 25, producing a crescent-shaped lumen (n = 3; Figure 2A). In the coronal plane, the initiating bulge gives the impression of a protrusion that divides the lumen of the intestine (Figure 2B). The protrusion is visible in the volume of interest (VOI) reconstruction as a longitudinal fold that projects into the lumen down the length of the intestine (Figure 2C, arrowhead). The protrusion within the lumen suggests the initiation of a vertical spiral, and we define this as a half turn as it does not create a 360° rotation in the lumen (Figure 2M).

Development of a spiral from the initial fold into the lumen occurs quickly after stage 25. In the skate, progression between stages is highly variable with some stages lasting 1-2 weeks, while others 4 or more weeks.[31] In addition, individual embryos can be variable in their progression through development and the batches of embryos we receive are not perfectly synchronized. Because individual stages can last several weeks and individual embryos are variable in their development, a collection received of single-stage embryos when incubated for 1 week can yield a range of stages from the original stage to 2 stages later. This makes capturing intermediate stages difficult. Stage 25 occurs 8-10 weeks postfertilization in our marine tanks, and stage 26 is reported to have a similar period of development.[31] In multiple attempts, we obtained only one stage 26 embryo. By microCT reconstruction, the stage 26 intestine contains a spiral with 2.5 spiral turns (personal observation). By stage 27, the crescent-shaped invagination is visible on transverse plane (n = 4; Figure D). The coronal view reveals how the crescent-shaped bulge is not a single event, but multiple turns running down the length of the intestine to divide the lumen into what appears like separate compartments in 2D view (Figure 2E). The 3D reconstruction of the intestine exposes a developing spiral with 4.5 rotations or turns within the lumen that is rotating in a right-handed orientation (Figure 2F,M).

At stage 30, the lobes of the liver extend caudally to fill the coelomic space, flanking either side of the spiral intestine (n = 4; Figure 2G,H). The fold that makes up the spiral has extended inward. The extension and tightening of the spiral correspond with a further compartmentalized lumen in the intestine. VOI rendering exhibits 6.5 turns to the spiral, corresponding with the 5+ compartments seen on coronal view and dataset video (Figure 2H,I, and Supporting Information Video S1). As observed on histological section, villi formation emerges after stage 30, and is present by stage 34 (n = 4; Figure 2J,K). By pre-hatching, the spiral fold has further elongated and tightened within the lumen, and the luminal compartments have enlarged. Villi line all surfaces of the spiral folds and the inner lining of the outer casing

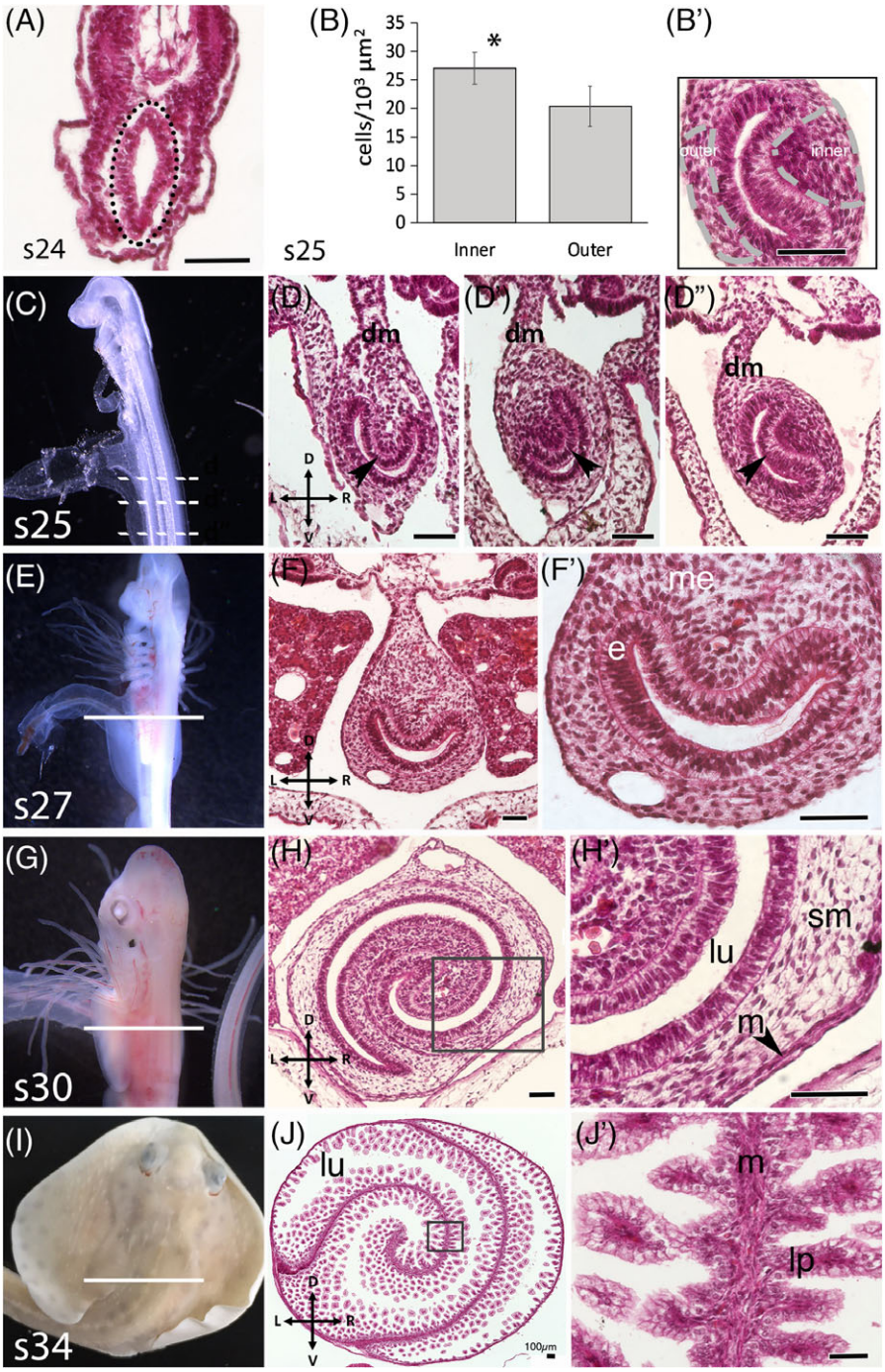

FIGURE 1 Developmental timeline for differentiation of the *Leucoraja erinacea* spiral intestine. A, A symmetric embryonic gut tube (dotted ellipse) is visible in a stage 24 embryo section stained for hematoxylin and eosin. B, Quantification of mesenchymal cell density at stage 25 in the inner and outer curvature bend of the intestinal lumen, as defined by the dashed lines on the section in (B′) (n = 9; $P = 0.003$). C,E,G,I, Images of whole-mount embryos used for histology and microCT scanning at stages 25, 27, 30, and 34, respectively. D-D″,F,F′,H,H′,J,J′, Transverse hematoxylin and eosin stained sections through the midline are indicated by the dashed white lines (C) and the solid white lines in corresponding stages (E,G,I). (D-D″) Section views through different positions of the rostral-caudal axis of a stage 25 embryo (C) show the gut tube is a simple epithelium surrounded by mesenchymal cells. A single asymmetric protrusion into the lumen appears in different positions relative to the dorsal mesentery along the length of the intestine (arrowheads). F, At stage 27, the embryonic gut tube has a pseudostratified epithelium is enclosed by mesenchyme that is loosely organized (F′). G,H, By stage 30, the spiral fold has elongated and tightened, folding in on itself creating a spiral-shaped lumen. H′, Magnified box in (H) shows the pseudostratified columnar epithelium surrounding the entire lumen with a clear basement membrane, submucosa and muscularis (arrowhead). J, Before hatching at stage 34, the spiral has further tightened turning inward 2 times. J′, The villi line both surfaces of the spiral fold, separated by a muscularis layer (boxed region in J). Scale bars = 50 µm in A,D-D″H-H″; 100 µm in J,J′. Abbreviations: dm, dorsal mesentery; e, epithelium; me, mesenchyme; sm, sub mucosa; m, muscle; lp, lamina propria; l, liver; lu, lumen

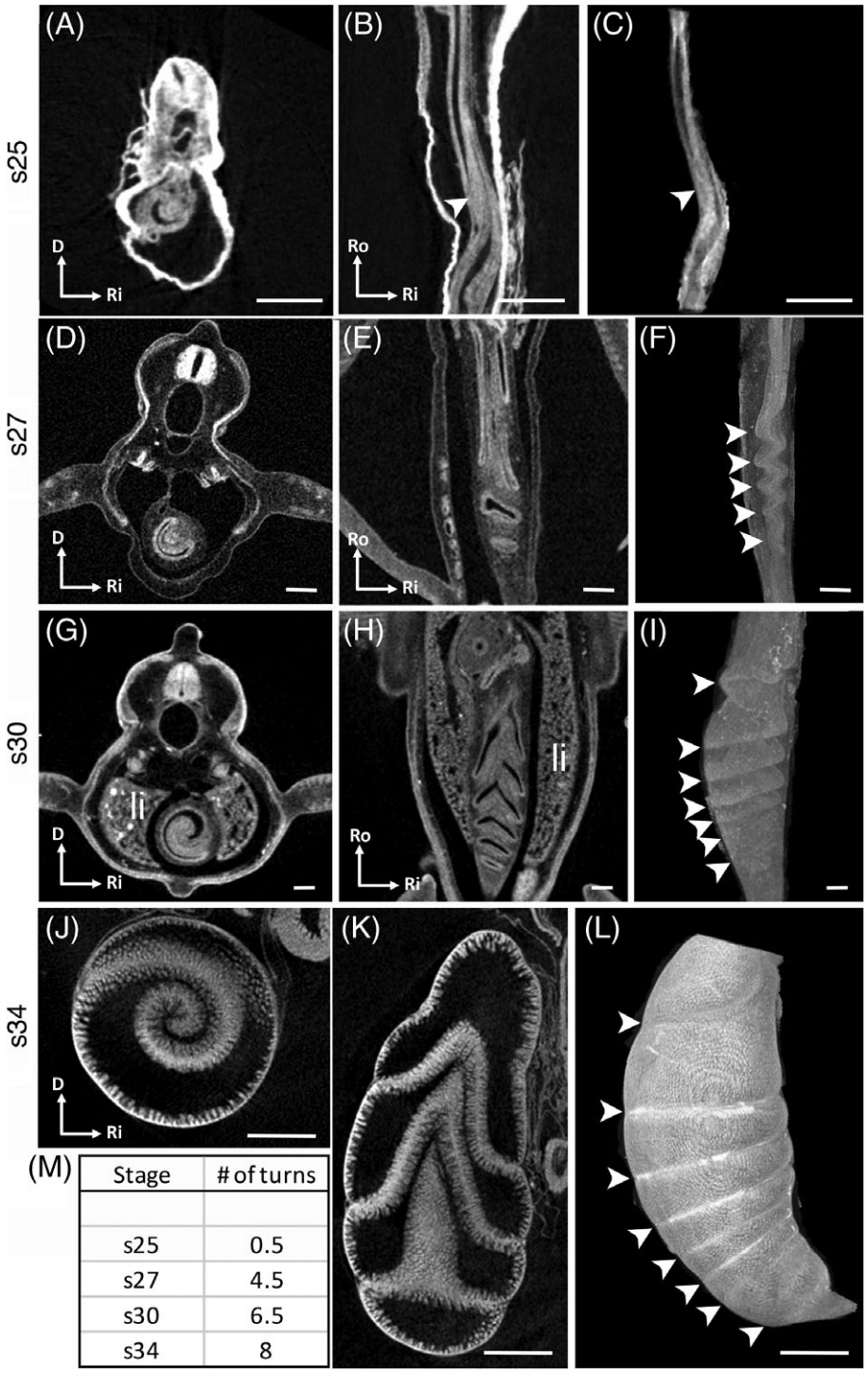

FIGURE 2 MicroCT scans and reconstructions reveal an increased number of spiral turns during development. A,D,G,J, Transverse plane images captured in Dataviewer of embryos scanned at stages 25, 27, 30 and 34, respectively. B,E,H,K, Coronal views through the midline of the spiral intestine at each stage. B, An invagination is visible at stage 25 (arrowhead). E,H, The number of folds within the intestinal lumen increases from stage 27 to 30. At stage 30, the left and right lobes of the liver have extended down the length of the intestine. K, At stage 34, villi are visible on all surfaces of the folds and inner surface of the outer intestinal wall. C,F,I,L, CTan VOI reconstructions from microCT datasets illustrate the 3D structure of the internal turns of the spiral (arrowheads). M, Summary of the number of turns within the spiral intestine at each developmental stage. Scale bars: 0.2 mm in A-I; 1 mm in J-L.
Abbreviations: D, dorsal; li, liver; Ri, right; Ro, rostral

(Figure 2K). Eight complete turns are evident on the 3D reconstruction (Figure 2L).

2.3 | Pitch length profiles during spiral development

To characterize the morphology of the spiral during intestine development, the pitch lengths between the turns of the internal spiral were measured and compared at different stages of development (Figure 3). Pitch length is defined as the distance between the edge of one turn of the spiral fold to the edge of the next complete turn (Figure 3G). As previously noted, the initial internal fold into the lumen at stage 25 we designated as a half turn, thus no pitch measurements were taken at this stage. At stage 27, the spiral has 4.5 turns, and pitch lengths do not change significantly from rostral to caudal pitch positions (1 through 4), (Figure 3A,B). Pitch lengths on the dorsal side ranged from 0.24 to 0.21 mm and 0.27 to 0.20 mm on

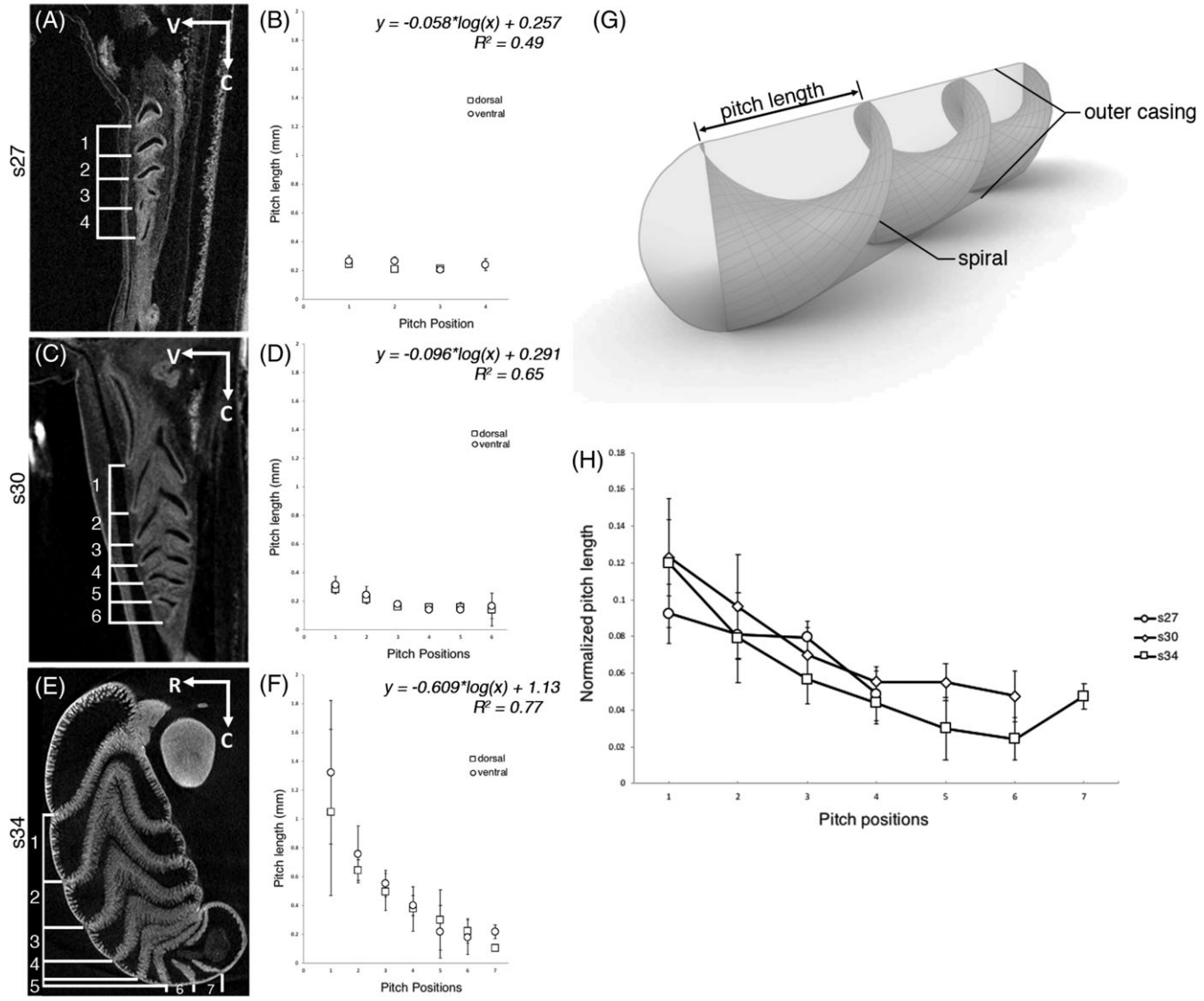

FIGURE 3 The profile of spiral pitch distances along the rostral-caudal axis changes during development. A,C,E, Sagittal microCT views of the developing spiral intestine from stages 27, 30, and 34, respectively. A,C, Images are oriented with ventral to the left, in (E) right is to the left, and the rostral to caudal axis runs top to bottom in all panels. Depicted in brackets are the pitch lengths that were measured between each turn of the spiral, numbered along the rostral-caudal axis. BD,F, The average pitch lengths between each pitch position are graphed adjacent to their corresponding image panels A,C,E, Every data point represents the mean pitch length (± SD) measured from the ventral and dorsal sides, respectively (stage 27, n = 3; stage 30, n = 4; stage 34, n = 4). ANOVA and regression analysis were performed using R (version 3.5). Independent regression slopes for Distance vs Stage are indicated on the graphs (stage 27, $P = 0.19$; stage 30, $P = 5.72 \times 10^{-6}$; stage 34, $P = 3.86 \times 10^{-7}$). G, Diagram of the spiral within the intestine (courtesy of C. Belmonte). The outer casing is defined as the outer walls of the intestine, and the fold twists within the lumen to make the spiral. Pitch length is the distance between the outer edge of two adjacent spiral rotations. H, Normalized pitch lengths are plotted as the mean pitch length divided by gut lengths (± SD) at each pitch position for stages 27 (n = 3), 30 (n = 4), and 34 (n = 4). ANOVA and regression analysis were performed ($R^2 = 0.7$, $P = 8.54 \times 10^{-15}$)
Abbreviations: C, caudal; R, right; V, ventral

the ventral side of the spiral pitch positions (n = 4). Because there are an incomplete number of turns at this stage, four pitch lengths were measured on the ventral side, while only three pitch lengths were calculable on the dorsal side. A linear regression demonstrates only a slight decrease in pitch length along the rostral-caudal axis of the spiral ($R^2 = 0.49$; $P = 0.19$). By stage 30, pitch lengths decrease significantly along the rostral to caudal axis (Figure 3C,D). Pitch lengths range from 0.28 to 0.14 mm on the dorsal side and 0.31 to 0.16 mm on the ventral side of the spiral pitch positions, respectively (n = 4). The slope of the linear regression shows a significant decrease at stage 30 compared with stage 27, meaning that the spiral is more tightly packed at the caudal end ($R^2 = 0.65$; $P = 5.72 \times 10^{-6}$). The steepest slope appears

TABLE 1 Summary of ANOVA analysis examining the effects of Stage, log-Pitch position, Dorsal/Ventral, and interactions between variables on pitch length

Variable	*P*-value
Stage	$\mathbf{3.17 \times 10^{-14}}$
Pitch position	$\mathbf{2.2 \times 10^{-16}}$
Dorsal, Ventral	0.613
Stage X Pitch position	$\mathbf{5.71 \times 10^{-9}}$
Stage X Dorsal/Ventral	0.333
Pitch position X Dorsal/Ventral	0.215
Stage X Pitch position X Dorsal/Ventral	0.282

Mean values were used for pitch lengths at stages 27 (n = 3), 30 (n = 4), and 34 (n = 4).

at stage 34, where pitch lengths decrease dramatically along the length of the spiral intestine with ranges of 1.0 to 0.10 mm on the dorsal and 1.3 to 0.22 mm on the ventral side, respectively (n = 4) (Figure 3E, f; $R^2 = 0.77$; $P = 3.86 \times 10^{-7}$).

Analysis of variance (ANOVA) analysis validated highly significant effects of different stages (Table : Stage) and different pitch positions (Table 1: Pitch length) on pitch lengths ($P = 3.17 \times 10^{-14}$ and 2.2×10^{-16}, respectively). Significant differences in pitch length were found comparing the position along the spiral at different stages (Stage X Pitch position, $P = 5.71 \times 10^{-16}$). No effect of dorsal vs ventral sides of the spiral was noted on pitch length (Dorsal/Ventral), on different stages (Stage X Dorsal/Ventral) or on pitch position along the spiral (Pitch position X Dorsal/Ventral) (Table 1).

To decouple pitch dynamics from global growth of the gut, we normalized pitch length to gut length for each stage. While stage 27 showed a different profile of pitch lengths compared with stages 30 and 34, ANOVA analysis revealed no significant difference between the normalized pitch lengths at different stages ($P = 0.22$) (compare Figure 3H). However, Pitch position does have a significant effect on pitch length ($P = 0.04$) and is dependent upon stage (Pitch position X Stage; $P = 0.005$).

2.4 | Helical angles in the developing spiral intestine

Along with pitch, a principal descriptor of spirals is the helical angles of the turn, defined as the angle between the fold of the spiral turn and a line perpendicular to the pitch. Examples of helical angles are illustrated for rostral-most spiral turns at stages 27, 30, and 34, respectively (Figure 4A,C,E). The helical angles show distinct trends at different developmental stages. At stage 27, helical angles along the rostral-caudal axis display a parabolic trend. The range of angles proceeds from 70° at the rostral end, down to 20° at the midpoint spiral turn number 3, and back up to 51° at the caudal end (Figure 4B). Linear regression of the log(Spiral turns) does not demonstrate a significant difference in the helical angles at this stage (Figure 4B; $R^2 = 0.09$; $P = 0.33$). In contrast, helical angles indicate a 3rd order polynomial trend along the length of the spiral at stage 30 with a peak of 58° at spiral turn 2, and a trough of 6° at turn 7 (Figure 4D). Linear regression confirms this trend is significant ($R^2 = 0.64$; $P = 7.49 \times 10^{-6}$). By stage 34, the trend in helical angles along the rostral-caudal axis appears to have flattened but maintains a polynomial curve with a peak of 33° at turn 2 and a low of 18° at turn 6 (Figure 4F). The trend of helical angles along the rostral-caudal axis at stage 34 is significant ($R^2 = 0.4$; $P = 6.73 \times 10^{-4}$). Thus, the spiral appears to become more uniform along the rostral-caudal axis over developmental time.

Examining the effects of Stage and log-Spiral turns by ANOVA analysis, we found that Spiral turns has a significant effect on helical angle, but there was no significant interaction with Stage or Stage X Spiral turn (Table 2).

2.5 | Coiling of the spiral during development

To elucidate the relationship of epithelial growth surrounding the lumen and radial constraints of the intestinal tube during spiral development, we examined the relationship between perimeter of the lumen and circumference of the gut tube along the rostral-caudal axis of the intestinal region (Figure 5). At stage 27, the perimeter is half the length of the circumference at the rostral turn, and this ratio decreases linearly toward the caudal end of the intestine (Figure 5B). By stage 30, the perimeter:circumference (P:C) ratio is equal, increases slightly at the midpoint and decreases at the caudal end. Stage 34 has a similar profile to stage 30, with a P:C starting greater than 1 at the rostral end. ANOVA analysis shows an effect of Stage and the intestinal rostral-caudal position independently on P:C (Stage, $P = 0.003$; log[Turns], $P = 0.04$). The effect of the position along the rostral-caudal axis also depends on the stage to a large degree ($P = 0.06$).

3 | DISCUSSION

3.1 | Initiation of a spiral

The progression of spiral formation and cell differentiation in the *Leucoraja erinacea* intestine provides clues as to how the spiral initiates. Before closure of the ventral body wall and narrowing of the embryonic gut tube into an umbilicus, the gut tube is symmetric at stage 24 (Figure 1A). Asymmetry within the developing intestine occurs at stage 25 and is marked by a protrusion that runs the length of the intestine (Figures 1D-D″, and 2A-C). The protrusion is an outgrowth of mesenchymal cells that bulges, causing the epithelium to bend outward and

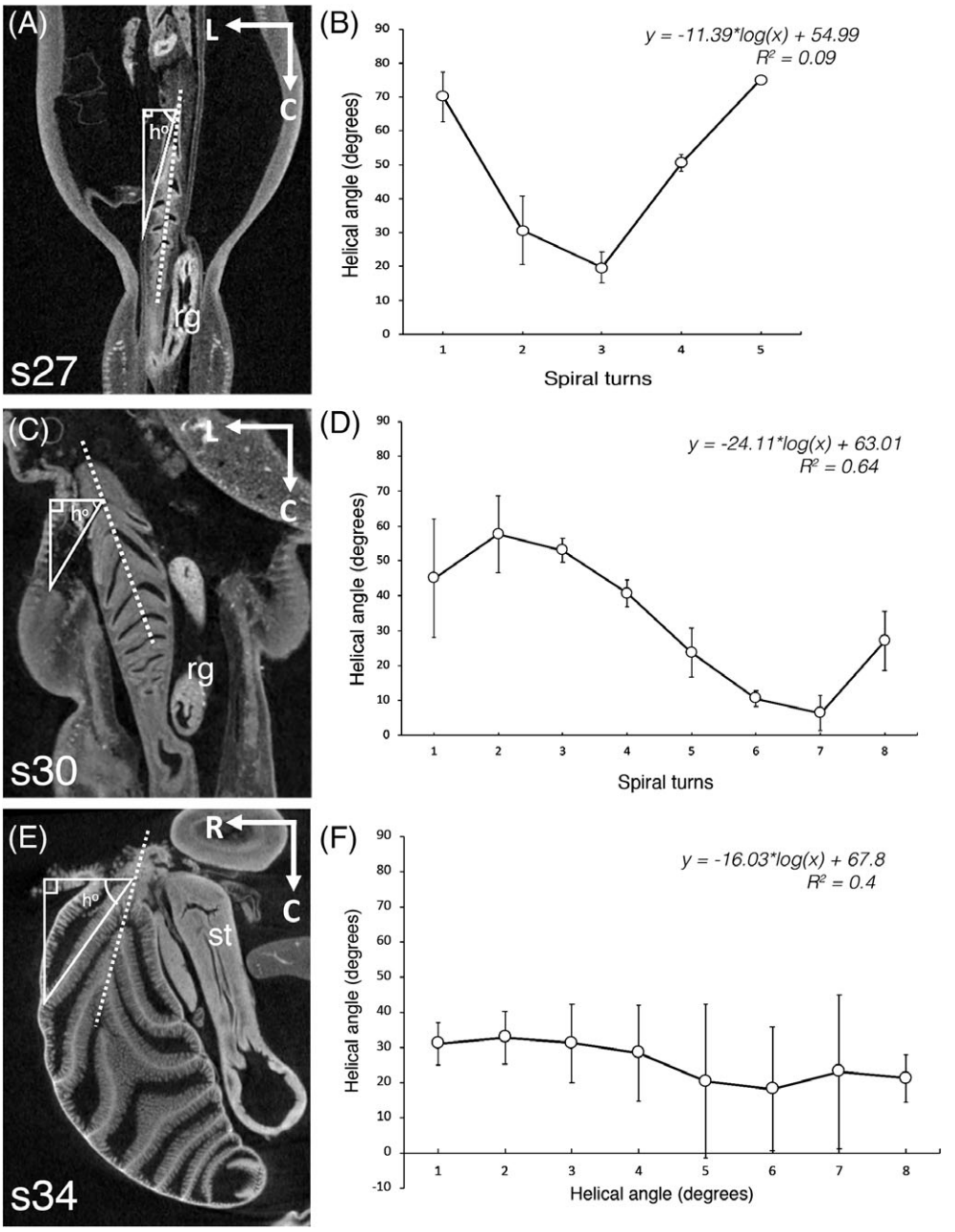

FIGURE 4 The profile of helical angles changes over developmental time. A,C,E, Coronal views of microCT scans captured in Dataviewer for stages 27, 30, and 34, respectively. Images are oriented with rostral-side up; the stomach marks the left and rectal gland the right sides of the abdominal cavity, respectively. Midlines for the rostral ends of the spiral intestine (dotted lines) were used to orient and measure the helical angles (h°). Midlines were reoriented moving caudally as the spiral intestines do not lie straight or flat in the body. B,D,F, Graphs of helical angles from rostral (spiral turn 1) to caudal for each corresponding stage in adjacent image panel. Every data point represents a mean helical angle (± SD) measured from the right side of the spiral as indicated by the triangles (stage 27, n = 3; stage 30, n = 4; stage 34, n = 3). Independent regression slopes were generated for Helical angle vs Spiral turns using R (version 3.5) by ANOVA and regression analysis (stage 27, $P = 0.33$; stage 30, $P = 7.49 \times 10^{-6}$; stage 34, $P = 6.73 \times 10^{-4}$). Abbreviations: C, caudal; L, left; rg, rectal gland; R, right; st, stomach

form a crescent-shaped lumen. The 1.3:1 ratio in mesenchymal cell density between the inner and outer curvature of the crescent suggests that the asymmetry may arise as a result of changes in cell shape and cell proliferation (Figure 1B).

TABLE 2 Summary of ANOVA analysis examining the effects of Stage and log-Spiral turns on helical angles using stages 27 (n = 3), 30 (n = 3), and 34 (n = 3)

Variable	P-value
Stage	0.322
Spiral turns	$\mathbf{1.38 \times 10^{-7}}$
Stage X Spiral turns	0.471

The break in symmetry is observed simultaneously at different orientations relative to the dorsal mesentery along the length of the developing intestine (Figure 1D-D″). Thus, while the asymmetric morphology is reminiscent of that seen in the generation of the stomach curvature, it is not clear whether this asymmetry is related to left-right (LR) identity.[32]

Naïve cells make up the epithelium and mesenchyme suggesting a rapid growth phase of the gut tube at this stage. Indeed, this rapid growth phase is reflected by the 4.5 spiral rotations seen at stage 27 (Figure 2F). From stages 25 to 27, the endoderm is a pseudostratified epithelium surrounded by loosely organized mesenchyme (Figure 1D′,F′). Together, this evidence suggests that spiral formation is initiated by induction of asymmetric growth within the

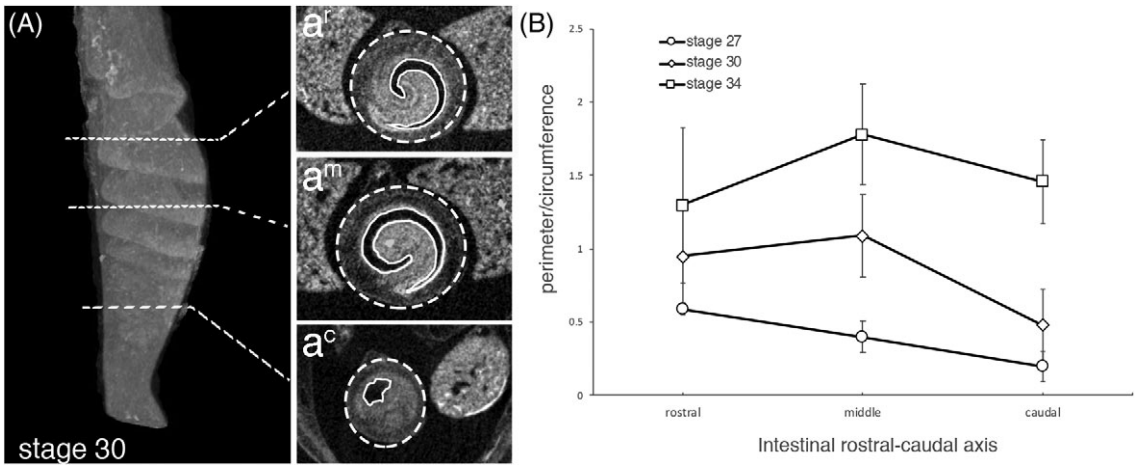

FIGURE 5 Rostral-caudal progression of spiral formation during development. A, VOI rendering of a stage 30 spiral intestine indicating the transverse views from which measurements were taken. The dashed lines depict the transverse views from the rostral (a^r), middle (a^m), and caudal (a^c) ends of the spiral intestine illustrating where the perimeter and circumference were measured. P:C ratio was calculated by dividing the perimeter (solid line) and circumference (dashed line) lengths. B, Graph of the mean (± SD) P:C ratios for rostral, middle and caudal regions of the spiral intestine at stages 27, 30 and 34. ANOVA and regression analysis were performed ($R^2 = 0.71$, $P = 5.6 \times 10^{-8}$)

mesenchyme and that the subsequent growth phase enables spiraling before cell differentiation.

3.2 | Development of a spiral

Once initiated by a single fold protruding into the lumen, the spiral rapidly progresses to 4.5 rotations in stage 27, to 6.5 rotations in stage 30, and finally 8 full rotations observed before hatching (Figure 1M). Thus, the most rapid spiraling occurs between stages 25 and 27. Progression from stages 25 to 27 occurs within the same timeframe (10-11 weeks post fertilization), and we were unable to consistently capture stage 26 for analysis. It would be interesting to attain several stage 26 embryos to better determine early progression of spiral formation. The rapid progression of spiral formation in the intestine between stages 25 and 27 necessitates an effort to generate a more accurate staging for embryonic gut development in *Leucoraja erinacea.*

Cell differentiation proceeds with a corresponding decreasing rate of spiral turn formation. In contrast to the rapid progression from stages 25 to 27, it takes approximately 2 to 4 weeks for embryos to progress from stages 27 to 30, and embryos can stay at stage 30 for up to 10 weeks. During this time, only 2 additional turns are included in the spiral, and the pseudostratified epithelium is surrounded by submucosa and muscularis regions (Figures 1H′ and 2 M). During the final stages of development before hatching, the number of spiral turns increases to eight complete rotations (Figure 2L). At stage 34, more than 14 weeks after stage 30, the walls of the intestine and spiral folds have thinned considerably and are comprised of distinct lamina propria and muscle fibers, and surfaces are surrounded in villi (Figure 1J,J′). Thus, after detection of the initial spiral fold at stage 25, spiraling occurs rapidly at first, and slows down as cell differentiation progresses through the later stages of development.

3.3 | Morphometry implicates role for physical forces in shaping the spiral

The role of physical forces in driving morphogenesis has appeared repeatedly in evolution to give rise to a diversity of shapes, including lung branching, brain folds, as well as intestinal loops and villi formation.[26,29,33–35] Morphometric analysis provides insights into how physical constraints may play a role in shaping spiral formation. At stage 27, the distance (pitch length) between each turn does not change significantly along the rostral caudal axis (Figure 3B). The equidistant spacing between the rotations of the spiral is conserved on both the dorsal and ventral sides, suggesting that any physical constraints exerted during gut development are equally distributed along the rostral-caudal axis of the gut tube, despite the fact that the spiral initiates with an asymmetric protrusion into the lumen.

During development, the rostral end of the spiral continues to lengthen, while the caudal end remains more constant. For example, the distance or length of pitch #1 is twice as long as the shortest pitch length (#4) at stage 30, and 10 times the length between pitch #1 and the shortest pitch length (#7) by stage 34 (Figure 3D,F). However, when compared directly and normalized for total gut length, there does not appear to be a significant difference in the profile of the pitch lengths between different stages (Figure 3H). This suggests that the change in spacing between the spiral turns reflects a global growth of the intestine tube during development, rather than progressive changes in the morphology of the spiral itself.

Simultaneously, the profile of helical angles at stage 27 displays a parabolic trend, with the largest helical angles at the rostral and caudal ends of the intestine (pitches 1 and 4, respectively) and the smallest helical angle at pitch 3 (Figure 4B). This means that the shape of the spiral appears more perpendicular to the midline in the middle of the intestine and folded downward at the rostral end at stage 27. This may suggest that, while overall there are consistent constraints along the length of the intestine, any twisting is initiated at the rostral end likely in conjunction with the turning of the stomach.

At later stages, helical angles display polynomial trends (Figure 4D,F). Consistent, the smallest helical angles correspond with the shortest pitch lengths at stage 30. As pitch lengths continue to increase at the rostral end by stage 34, helical angles become more constant along the rostral-caudal axis (Figure 4F). The decreasing pitch distances from rostral to caudal supports that rotation of the spiral fold likely initiates on the rostral end near the stomach, resulting in a longer pitch length. This would be consistent with getting sequentially smaller pitch lengths toward the caudal end, and more consistent helical angles at later stages and more variable angles earlier. Furthermore, the skate spiral reflects the trend of anterior-posterior (or rostral-caudal) progression of morphogenesis in amniotes.[35,36]

The possible role of constraints during spiral formation is revealed when we examine the P:C relationship during development (Figure 5). At stage 27, the P:C ratio decreases linearly from along the rostral to caudal axis. In contrast, the P:C ratio increases at the midpoint of the intestine at stages 30 and 34 (Figure 5B). The P:C ratio also increases significantly with progressing stages. Together, we deduce that points of constraints on the developing gut tube change between stages 27 and later stages, and that these constraints increase overall through development. Furthermore, we propose that radial constraints from the outer casing of the gut tube play a role in spiraling. The increase in the number of spiral turns during development may be the result of both constraints imposed by differentiating smooth muscle in the outer casing, and growth and elongation of the spiral folds.[26]

3.4 | Model for spiral initiation and growth in the little skate

Based on the evidence presented, we propose a preliminary model for spiral initiation and growth in the little skate intestine (Figure 6). Appearance of a spiral fold initiates as an asymmetric focus of growth within the mesenchyme that protrudes into the lumen and runs the length of the early intestinal gut tube at stage 25. This primary protrusion or fold expands at a greater rate than adjacent tissues such as the dorsal mesentery, resulting in constraining forces that likely cause the internal fold in the tube to twist forming a visible spiral by stage 27. As the intestine increases in overall length, the inner fold making up the spiral continues to grow and extend through later stages, turning inward upon itself (Figure 2G,J). The inward spiral of the folds and consequent increase in the number of spiral turns (eight when completed) likely results from a second set of constrictive forces possibly resulting from the differentiation of smooth muscle in the outer casing of the intestine. It is not yet clear how these forces may affect the handedness of the spiral.

The source of constraining forces maybe due to asymmetries marked by the LR identity. Activation of the Nodal cascade on the left side of the embryo results in asymmetric organ morphologies and in organ rotation.[37,38] The Nodal target gene *Pitx2* is expressed on the left-side of developing organs and directs cell shape changes that lead to asymmetric organ morphologies in the gut.[32,39,40] In addition, *Pitx2* directs cell shape changes in the dorsal mesentery that control the direction of gut looping.[27,28] Of interest, the break in symmetry observed at stage 25 is not strictly a LR event, as the

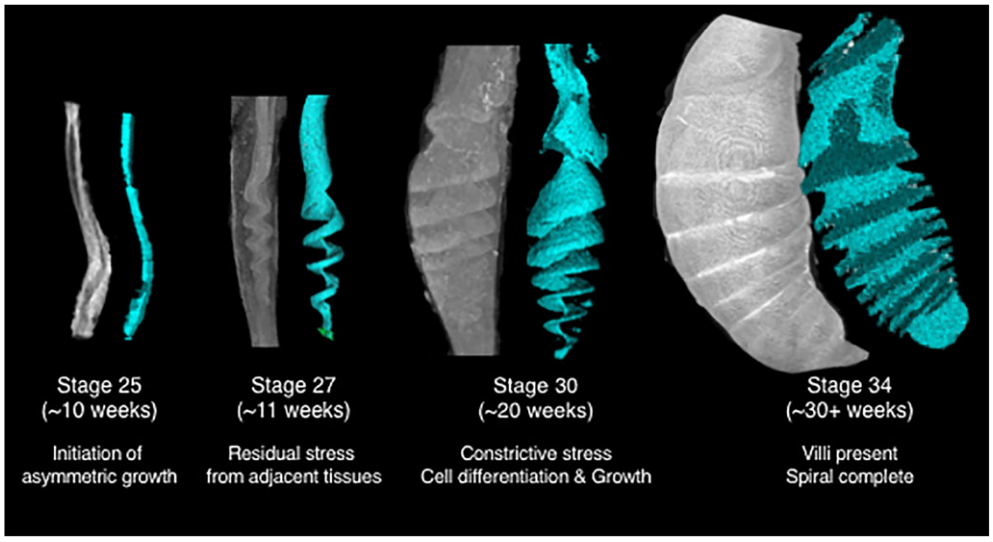

FIGURE 6 Proposed model for spiral formation. Schematic showing the volumetric reconstructions of the spiral intestine adjacent to the 3D renderings of the spiral lumen contained within the intestine at different stages of development

asymmetric curvature occurs at different orientations relative to the dorsal mesentery along the length of the intestine (Figure 1D-D″). While the established and conserved role of *Pitx2* in directing asymmetries in organ shape and positioning leads us to propose that the constrictive forces that drive spiral formation are likely downstream of *Pitx2*, further investigation is warranted to establish the connection between the asymmetric curvature in the spiral intestine and LR identity.

Previous work has highlighted the roles of mechanical forces and differential growth on the geometry of gut looping.8,[26,29] Our present work suggests that the same principles apply to the developing spiral intestine in *Leucoraja erinacea.* The spiral intestine may itself be an extreme example of the combination of differential growth between the gut tube and surrounding tissues, and residual constrictive stress generated within the gut tissue generating a truly unique geometric structure.

4 | EXPERIMENTAL PROCEDURES

4.1 | Animals

Leucoraja erinacea (little skate) egg cases were obtained from the Woods Hole Marine Biological Laboratory (Woods Hole, MA), and cultivated in circulating salt-water tanks with reconstituted Instance Ocean (Aquarium Systems) at 16°C with a 12-hr light-dark cycle. Eggs maintained at a constant temperature can take approximately 12 months to hatch, or as long as 22 months at temperatures fluctuating below 10°C.[31,41] Embryos were staged based on the number of branchial arches, and the size and shape of the mouth and pectoral fins according to corresponding stages described for the winter skate, *Leucoraja ocellate.*[31] Embryos harvested at stages 24, 25, and 27 were removed from their egg cases, and fixed in 4% paraformaldehyde, while late staged embryos (stages 30 and 34) were first killed with MS-2222 (Sigma-Aldrich) before fixation. Fixation in 4% paraformaldehyde occurred by shaking for 24 to 48 hr at 4°C. Embryos were rinsed in phosphate buffered saline (PBS) (3 × 15 min) at room temperature and dehydrated to 70% ethanol through a graded series of 15 to 30 min rocking incubations (25%, 50%, 70% in 1× PBS). Embryos used for scanning were stored at −20°C, while those used for histology were transferred to glass scintillation vials and further dehydrated to 100% ethanol. All procedures for animal care and use were in accordance with the standards set by the NIH and approved by the Institutional Animal Care and Use Committee at Union College.

4.2 | Histology and cell density

Embryos used for histology were cleared by washing twice in xylene for 5-15 min, depending on the stage, and embedded in paraffin. Transverse 6-μm sections were cut and dried overnight at 37°C. Slides were stained with hematoxylin and eosin following standard procedures.[42] To quantify cell density on either side of the crescent-shaped lumen at stage 25, the area of the inner and outer curvature (as highlighted in Figure 1B′) was calculated using the SPOT 5.0 software. The number of cells within the inner and outer curvature areas were determined by manually counting nuclei. Counts were performed in triplicate, averaged, and divided by area to calculate the number of cells per 1000 μm^2.

4.3 | MicroCT scanning

Fixed, embryos dehydrated to 70% ethanol were stained in phosphotungstic acid (PTA) solution (1% phosphotungstic acid in water, mixed to 30% PTA in 70% ethanol) for 12 to 48 hr rocking at 4°C as previously described.[43,44] To facilitate penetration of fixative at later stages, stage 30 and 34 embryos were trimmed with a razor blade, leaving the abdominal cavity, and stained in PTA for up to 7 days rocking at 4°C. After staining, embryos were washed twice in 70% ethanol, twice in 100% ethanol, rocking at room temperature for 15 min each, and stored in −20°C until scanned. For scanning, embryos were mounted inside a pipette tip that had the tip-end flamed closed and the wide end cut off with a razor blade. The pipette tip was fitted tip-side down into a piece of foam and filled with 100% ethanol. Embryos were placed caudal end down toward the tip, and the wide end was sealed with paraffin.

Embryos were scanned at Union College using a SkyScan 1272 scanner (Brucker). Scans were performed at a pixel resolution of 4 k at 70 kV and a 0.5 mm aluminum filter. Multiple scans were performed for stages 25 (n = 3), 27 (n = 4), 30 (n = 4), s34 (n = 4), and scanning parameters are further specified (Table 3). Resulting scan sets were reconstructed in NRecon software. Reconstructions of the VOI renderings of the developing spiral intestine were made in CTan software, and CloudCompare was used to generate 3D models. In CloudCompare, the outer intestinal casing was subtracted manually to reveal the inner spiral.

4.4 | Morphometric analysis

The pitches and helical angles of micro-CT scanned intestines from developmental stages 27, 30, and 34 were measured to determine the extent to which spiral folding varies throughout the gut tube. For pitch measurements, data sets were saved in the sagittal plane in DataViewer. Once opened in CTan, the datasets were in proper orientation for measuring pitches in the sagittal plane. The gut midline was found by averaging the outer data lines for the edges of the intestinal walls. From the midline sagittal plane, pitch was measured. Pitch, the distance between the outer edge of each turn

TABLE 3 MicroCT scan parameters for *Leucoraja erinacea* embryos used in this study

Stage	# Scanned	μA	Exposure time	Voxel size μm^3	Resolution
25	3	142	2 s	27.3	3.01 μm
		142	2 s	27.3	3.01 μm
		142	2 s	27.3	3.01 μm
27	4	142	2 s	27.3	3.01 μm
		142	2 s	27.3	3.01 μm
		142	2 s	27.3	3.0 μm
		142	2 s	29	3.07 μm
30	4	142	2 s	42.1	3.48 μm
		142	2 s	44.4	3.54 μm
		142	2 s	27.3	3.01 μm
		142	2 s	27.3	3.01 μm
34	4	142	1.3 s	1000	10 μm
		130	1.6 s	125.8	5.01 μm
		142	1.3 s	153.1	5.35 μm
		130	2.8 s	131.1	5.08 μm

in the spiral was measured in CTan with the distance tool (Figure 3A,C,E). Pitch lengths (μm) were obtained from both dorsal and ventral sides of the intestine for every individual turn at the midline and three points above and three points below the midline, for an average of the distance between each turn. Average pitch lengths for the dorsal and ventral sides were plotted for each stage (Figure 3B,D,F). To normalize pitch length data between stages, overall gut lengths for each gut were measured in CTan, and pitch lengths were divided by gut lengths, averaged for each position and plotted (Figure 4).

Helical angles were measured for each spiral fold in respect to the spiral midpoint. Midpoints were determined in Dataviewer by orienting the curser to the center of the spiral in the transverse plane, which was reflected in the corresponding coronal section to find the midpoint. The midpoint for the spiral determined the midline axis. The helical angle was defined as the angle from the midline axis to a tangent line determined by the apex of the spiral fold on the left side of the body (Figure 5A,C,E). Angles were manually measured using a protractor, as the angle tool in CTan did not work well with the orientation of the coronal view of the spirals. For stages 30 and 34, the spiral intestine is curved within the body axis. To collect accurate and consistent measurements, multiple midline axes were determined for each spiral fold down the length of the intestine. Averages of helical angles for each spiral turn were graphed (Figure 5B,D,F).

To quantify coiling of the spiral during development, measurements of the perimeter of the lumen and gut circumference were made in CTan at stages 27, 30, and 34. The measurements were taken at the rostral-most turn of the spiral, the middle, and at the caudal-most or final turn of the spiral intestine for each scanned embryo. Means of perimeter divided by circumference for each positional measurement at the different stages were graphed (Figure 6).

4.5 | Statistical analysis

Pitch lengths and helical angles were examined to explore relationships between spiral turns within the same stage or between different developmental stages. Average pitch lengths for the dorsal and ventral sides of each pitch position were plotted at stages 27, 30, and 34, respectively. We used linear regression to look at the relationship between the log-pitch position for each spiral turn, and pitch length. Separate regressions were performed for each developmental stage using R (version 3.5). Measurements for helical angles were treated similarly. Average helical angles were plotted for each spiral turn at the different developmental stages. Separate linear regressions were run to examine the relationship of log-spiral turns on helical angles.

To determine variables effecting differences in pitch length, we analyzed the independent variables Stage, Pitch position, and Dorsal/Ventral separately by ANOVA. Interactions between the independent variables including Stage X Pitch position, Stage X Dorsal/Ventral, Pitch position X Dorsal/Ventral and Stage X Pitch position X Dorsal/Ventral were examined. Similar analysis was repeated with normalized pitch length data, examining interactions between the independent variables Stage, Pitch position, and Stage X Pitch position. We also compared the effect of Stage and Spiral turns on helical angles, separately and in combination (Stage X Spiral turns). Interactions between independent

variables (Stage X Spiral turns) were assessed for their effects on coiling of the spiral (perimeter:circumference).

ACKNOWLEDGMENTS

Research is rewarding because of the contributions of great thought partners. We thank N. Nerurkar (Columbia University) and J. Corbin (Union College) for their discussion of the data and expertise in using R, respectively, and C. Belmonte (Union College) for the diagram image in Figure 3G. We are grateful to several talented undergraduates who have assisted with technical support: Alexis Wojtowicz, Jordan deFelice, and Samantha Frye. Embryos were scanned on a SKYSCAN1272 microCT scanner supported by NSF-MRI #1531850, and 3D reconstructions were printed with support from NSF-MRI #1337768.

ORCID

Nicole A. Theodosiou https://orcid.org/0000-0002-0043-383X

REFERENCES

1. Kilner PJ, Yang G-Z, Wilkes AJ, Mohiaddin RH, Firmin DN, Yacoub MH. Asymmetric redirection of flow through the heart. *Nature*. 2000;404:759-761.
2. Aylsworth AS. Clinical aspects of defects in the determination of laterality. *Am J Med Genet*. 2001;101:345-355.
3. Ramsdell AF. Left-right asymmetry and congenital cardiac defects: getting to the heart of the matter in vertebrate left-right axis determination. *Dev Biol*. 2005;288:1-20.
4. Stewart DR, Colodny AL, Daggett WC. Malrotation of the bowel in infants and children: a 15 year review. *Surgery*. 1976;79:716-720.
5. Burn SF, Hill RE. Left-right asymmetry in gut development: what happens next? *Bioessays*. 2009;31:1026-1037.
6. Sutherland MJ, Ware SM. Disorders of left-right asymmetry: heterotaxy and situs inversus. *Am J Med Genet C Semin Med Genet*. 2009;151C:307-317.
7. Burdine R, Schier A. Conserved and divergent mechanisms in left-right axis formation. *Genes Dev*. 2000;14:763-776.
8. Nerurkar NL, Mahadevan L, Tabin CJ. Bmp activity controls forces in gut looping. *Proc Natl Acad Sci U S A*. 2017;114:2277-2282.
9. Nickel R, Schummer A, Seiferle E. *Lehrbuch der Anatomie der Haustiere*. Stuttgart: Parey Publishers; 1995.
10. Grande C, Patel NH. Lophotrochozoa get into the game: the nodal pathway and left/right asymmetry in bilateria. *Cold Spring Harb Symp Quant Biol*. 2009;74:281-287.
11. Kuroda R, Endo B, Abe M, Shimizu M. Chiral blastomere arrangement dictates zygotic left-right asymmetry pathway in snails. *Nature*. 2009;462:790-794.
12. Blum M, Feistel K, Thumberger T, Schweickert A. The evolution and conservation of left-right patterning mechanisms. *Development*. 2014;141:1603-1613.
13. Wetherbee BM, Gruber SH, Cortes E. Diet, feeding habitats, digestion, and consumption in sharks with special reference to the Lemon Shark, *Negaprion brevirostris*. In: Pratt HL, Gruber SH, Taniuchi T, eds. *"Elasmobranchs as Living Resources" Advances in the Biology, Ecology, Systematics, and Status of Fisheries*. Washington, DC: US Department of Commerce; 1990.
14. Moss SA. *Sharks*. Englewood Cliffs, NJ: Prentice-Hall Inc; 1984:246.
15. Karachle PK, Stergiou KI. Gut length for several marine fish: relationships with body length and trophic implications. *Mar Biodivers Rec*. 2010;3:e106.
16. Baldridge HD. Sinking factors and average densities of Florida sharks as functions of liver buoyancy. *Copeia*. 1970;1970:744-754.
17. Hassanpour M, Joss J. Anatomy and histology of the spiral valve intestine in juvenile Australian lungfish, *Neoceratodus forsteri*. *Open Zoology J*. 2009;2:62-85.
18. Argyriou T, Clauss M, Maxwell EE, Furrer H, Sanchez-Villagra MR. Exceptional preservation reveals gastrointestinal anatomy and evolution in early actinopterygian fishes. *Sci Rep*. 2016;6:18758.
19. Theodosiou NA, Hall DA, Jowdry AL. Comparison of acid mucin goblet cell distribution and Hox13 expression patterns in the developing vertebrate digestive tract. *J Exp Zool B Mol Dev Evol*. 2007;308:442-453.
20. Theodosiou NA, Simeone A. Evidence of a rudimentary colon in the elasmobranch, *Leucoraja erinacea*. *Dev Genes Evol*. 2012;222:237-243.
21. Jaffe MJ, Galston AW. The physiology of tendrils. *Annu Rev Plant Physiol*. 1968;19:417-434.
22. Grande C, Patel NH. Nodal signalling is involved in left-right asymmetry in snails. *Nature*. 2009;457:1007-1011.
23. Bayly PV, Taber LA, Kroenke CD. Mechanical forces in cerebral cortical folding: a review of measurements and models. *J Mech Behav Biomed Mater*. 2014;29:568-581.
24. Kuhl E. Growing matter: a review of growth in living systems. *J Mech Behav Biomed Mater*. 2014;29:529-543.
25. Razavi MJ, Wang X. Morphological patterns of a growing biological tube in a confined environment with contacting boundary. *RSC Adv*. 2015;5:7440-7449.
26. Shyer AE, Tallinen T, Nerurkar NL, et al. Villification: how the gut gets its villi. *Science*. 2013;342:212-218.
27. Davis NM, Kurpios NA, Sun X, Gros J, Martin JF, Tabin CJ. The chirality of gut rotation derives from left-right asymmetric changes in the architecture of the dorsal mesentery. *Dev Cell*. 2008;15:134-145.
28. Kurpios NA, Ibanes M, Davis NM, et al. The direction of gut looping is established by changes in the extracellular matrix and in cell:cell adhesion. *Proc Natl Acad Sci U S A*. 2008;105:8499-8506.
29. Savin T, Kurpios NA, Shyer AE, et al. On the growth and form of the gut. *Nature*. 2011;476:57-62.
30. Grosse AS, Pressprich MF, Curley LB, et al. Cell dynamics in fetal intestinal epithelium: implications for intestinal growth and morphogenesis. *Development*. 2011;138:4423-4432.
31. Maxwell EE, Frobisch NB, Heppleston AC. Variability and conservation in late chondrichthyan development: ontogeny of the winter skate (*Leucoraja ocellata*). *Anat Rec (Hoboken)*. 2008;291:1079-1087.

32. Davis A, Amin NM, Johnson C, Bagley K, Ghashghaei HT, Nascone-Yoder N. Stomach curvature is generated by left-right asymmetric gut morphogenesis. *Development*. 2017;144:1477-1483.
33. Wiggs BR, Hrousis CA, Drazen JM, Kamm RD. On the mechanism of mucosal folding in normal and asthmatic airways. *J Appl Physiol (1985)*. 1997;83:1814-1821.
34. Toro R, Burnod Y. A morphogenetic model for the development of cortical convolutions. *Cereb Cortex*. 2005;15:1900-1913.
35. Kimelman D, Martin BL. Anterior-posterior patterning in early development: three strategies. *Wiley Interdiscip Rev Dev Biol*. 2012;1:253-266.
36. Morris SA, Grewal S, Barrios F, et al. Dynamics of anterior-posterior axis formation in the developing mouse embryo. *Nat Commun*. 2012;3:673.
37. Nonaka S, Tanaka Y, Okada Y, et al. Randomization of left-right asymmetry due to loss of nodal cilia generating leftward flow of extraembryonic fluid in mice lacking KIF3B motor protein. *Cell*. 1998;95:829-837.
38. Levin M, Thorlin T, Robinson KR, Nogi T, Mercola M. Asymmetries in H+/K+-ATPase and cell membrane potentials comprise a very early step in left-right patterning. *Cell*. 2002;111:77-89.
39. Faucourt M, Houliston E, Besnardeau L, Kimelman D, Lepage T. The pitx2 homeobox protein is required early for endoderm formation and nodal signaling. *Dev Biol*. 2001;229:287-306.
40. Raya A, Izpisua Belmonte JC. Left-right asymmetry in the vertebrate embryo: from early information to higher-level integration. *Nat Rev Genet*. 2006;7:283-293.
41. Ballard WW, Mellinger J, Lechenault H. A series of normal stages for development of *Scyliorhinus canicula*, the lesser spotted dogfish (Chondrichthyes: Scyliorhinidae). *J Exp Zool*. 1993;267:318-336.
42. Allen T. Hematoxylin and eosin. In: Sobin L, ed. *Laboratory Methods in Histotechnology*. Washington, DC: American Registry of Pathology; 1994:53-57.
43. Metscher B. MicroCT for developmental biology: a versatile tool for high-contrast 3D imaging at histological resolutions. *Dev Dyn*. 2009;238:632-640.
44. Metscher BD. MicroCT for comparative morphology: simple staining methods allow high-contrast 3D imaging of diverse non-mineralized animal tissues. *BMC Physiol*. 2009;9:11.

SUPPORTING INFORMATION

Additional supporting information may be found online in the Supporting Information section at the end of this article.

How to cite this article: Theodosiou NA, Oppong E. 3D morphological analysis of spiral intestine morphogenesis in the little skate, *Leucoraja erinacea*. *Developmental Dynamics*. 2019;1–14. https://doi.org/10.1002/dvdy.34